Chapter 2

Observations and Data Analysis Techniques: Space and Ground-based Instruments

In this chapter, we outline a brief description of various space and ground-based observatories (e.g., Solar Dynamics Observatory *SDO;* ***Solar and Heliospheric Observatory*** *SOHO;* ***Solar TErrestrial RElations Observatory*** *STEREO;* ***Hinode; Global Oscillation Network Group*** *GONG;* ***Geostationary Operational Environmental Satellites*** *GOES,* ***etc). We also describe some details of instruments onboard these observatories, e.g., Atmospheric Imaging Assembly*** *AIA;* ***Sun-Earth Connection Coronal and Heliospheric Investigation*** *SECCHI* ***Coronagraphs and EUV Imager; Heliospheric and Magnetic Imager*** *HMI;* ***X-ray Telescope*** *XRT,* ***etc. We analyze the observational data from these instruments in the present thesis to study the coronal jets and their association with the CMEs. We also describe the data analysis techniques used in various works presented in this thesis, e.g., the calibration of EUV image data, magnetograms, and coronagraphic observations; Tie-Pointing Method to measure the most accurate distance-time***

diagram of solar eruptions in order to estimate their kinematics; Potential Field Source Surface (PFSS) Extrapolation of the Magnetic Fields; and Fourier Local Correlation Technique (FLCT) to estimate the photospheric optical flows at Sun. In the last section, We conclude about the importance of the analyzed observations and their analysis methods.

2.1 Introduction

The imaging observations in X-ray and Extreme Ultraviolet (EUV) wavelength range of the electromagnetic spectrum are utilized to probe the dynamics and properties of various layers of the million-degree hot solar atmosphere, which also provide a rich information on the concurrent eruptive phenomena (e.g., solar flares, coronal jets, CMEs) in the solar atmosphere. In the present thesis, we have used multi-wavelength imaging observational data to analyse the triggering mechanisms and properties of the coronal jets in different magnetic regions (e.g., active region and its boundary; quiet-Sun region). The coronagraphic observations are also utilized to study the CMEs associated with the jets.

The solar magnetogram observations are used to estimate the magnetic field strength in certain regions of the solar photosphere, which also provide an opportunity to measure the spatio-temporal variations of the magnetic fluxes. In this thesis, we have utilized the Helioseismic and Magnetic Imager (Scherrer *et al.*, 2012) to understand the nature, evolution, and changes of the magnetic fields at the footpoints of coronal jets to understand the role in their triggering. Generally, the coronal jets are localized transient phenomena that are most likely associated with the energy release in the solar atmosphere. Therefore, their evolution and properties can be studied in different EUV emissions from the ions at different ionization stages sensitive to the range of the temperatures in the solar atmosphere. We utilize the multi-wavelength EUV imaging observations captured from Atmospheric Imaging Assembly (AIA) onboard Solar Dynamics Observatory (Lemen *et al.*, 2012) to

understand the triggering, evolution, and eruption of a variety of coronal jets. The Coronal Mass Ejection (CME) phenomena is generally observed with the white light coronagraphs when they propagate in the outer diffused corona. In these coronagraphs, there are in-built occulting disk which cover whole solar disk. Large Angle Spectroscopic COronagraph (LASCO) onboard SOHO have three coronagraphs C1, C2, C3 which observe from 1.1 to 30 $R_{\odot}$ solar regions Brueckner *et al.* (1995). COR1 and COR2 coronagraphs of STEREO_A and STEREO_B (launched in 2006) observe CMEs from different positions and provide different view-points to analyze CMEs and also help in reconstruction of the 3D evolution of the CMEs (Howard *et al.*, 2008). STEREO spacecrafts are in elliptical heliocentric orbits. We utilize observations from these coronagraphs in understanding the physical origin and propagation properties of the CMEs/narrow-CMEs associated with various coronal jets. Apart from that, a variety of complementary observations are useful to understand the evolution of the different plasma components of the coronal jets as well as to observe any flaring activities in case happening at their base. In the purview of this, we have also used the observations of the jet emitting regions at the Sun in the frame-work of H-α (e.g., GONG (Harvey *et al.*, 2011)) and integrated soft X-ray light curves (e.g., GOES (Garcia, 1994) X-ray time series).

The multiwavelength solar imaging and magnetic observations need initial calibration to remove the artefacts and clean the data. Certain physical methods need to also be employed to derive the scientific information from the specific observational data sets. In the present thesis, we employ some advanced data analysis method, e.g., Potential Field Source Surface (PFSS) extrapolation; Fourier Local Correlation Tracking of the optical flows; and the Tie-Pointing method to triangulate the STEREO A & B images to exactly estimate the kinematics of the plasma ejecta. The details of these methods are presented in this chapter. In conclusions, in the present chapter, we briefly discuss the different space-based and ground-based observational instruments and their data which are used

for multi-wavelength study of coronal jets and other solar transients. We discuss about calibration and analysis techniques for processing the observational data. We conclude at the end the physical significance of the utilized observational data and their analysis techniques.

2.2 Solar Dynamics Observatory (SDO)

The Solar Dynamics Observatory (SDO) is the first mission of NASA's Living with a Star (LWS) Program (Lemen *et al.*, 2012). This space-weather mission was launched on 11 February 2010 and providing the scientific data from 01 May 2010. The SDO mission was launched to accomplish many scientific goals in understanding of the Sun e.g., develop space-weather predictability, topological magnetic field configuration, variations in solar spectral irradiance, prediction and internal processes of solar cycle. The SDO mission consists of three instruments namely the Atmospheric Imaging Assembly (AIA), Helioseismic and Magnetic Imager (HMI) and Extreme Ultraviolet Variability Experiment (EVE). Figure 2.1 shows the SDO mission and its different instruments. In the present thesis, we use AIA and HMI data to study different transient phenomena (e.g., coronal jets, flares, etc) which will be discussed in the forthcoming subsections.

2.2.1 Atmospheric Imaging Assembly (AIA)

AIA observes solar corona and transition region in multi-wavelengths high resolution filters. AIA has four multi-layered coated telescopes which are dual channelled and normal incidence (see Figure 2.2). AIA has 4 telescopes. AIA telescope 1 contains 131 Å and 335 Å , AIA telescope 2 contains 193 Å and 221 Å . AIA telescope 4 contains 94 Å and 304 Å . AIA telescope 3 contains 171 Å , 1600 Å , 1700 Å and 4500 Å . Telescope 3 has MgF2 window with centered coating at 1600 Å . These telescopes observe full disk Sun in

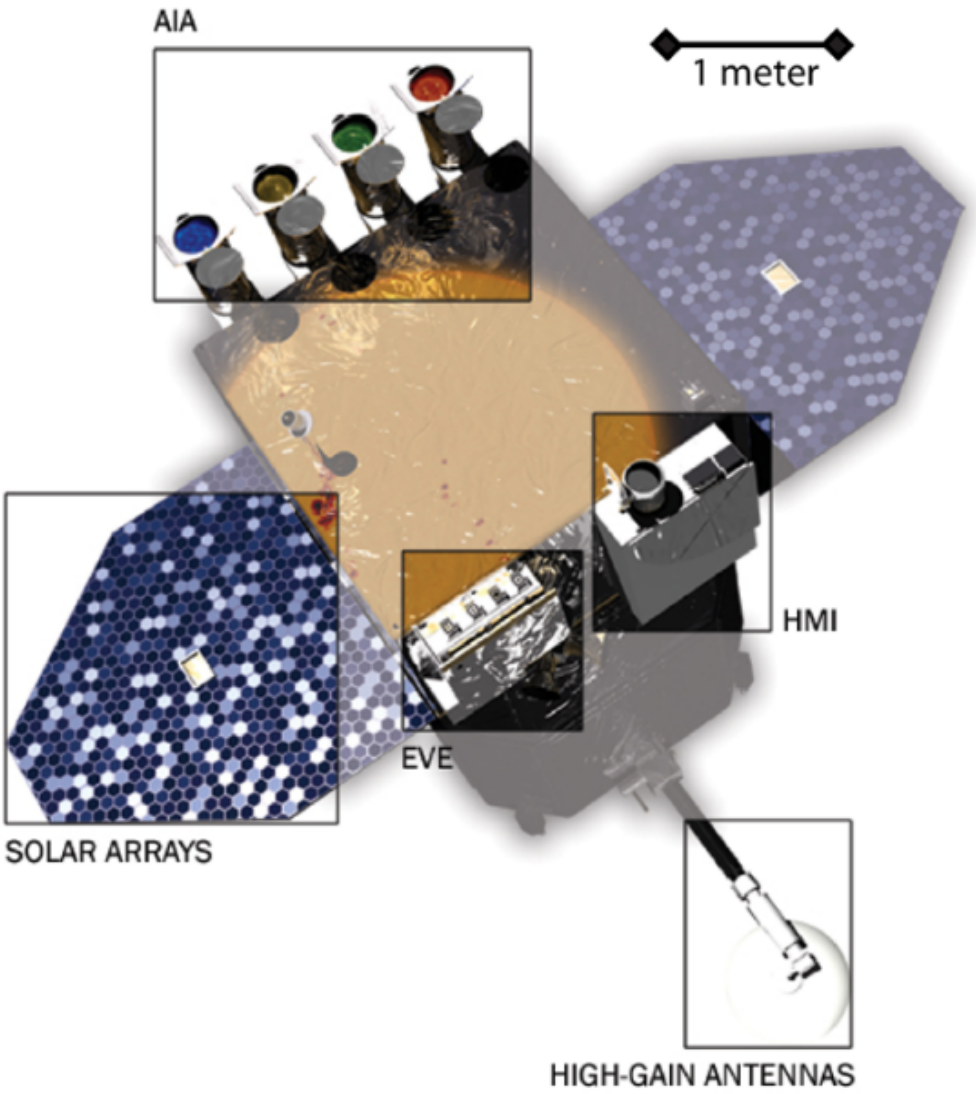

Figure 2.1: The SDO mission with all its instruments AIA, HMI, EVE, and solar arrays, high-gain antennas are also marked. Main engine of the satellite is on another side. (Courtesy: Pesnell, Thompson and Chamberlin (2012))

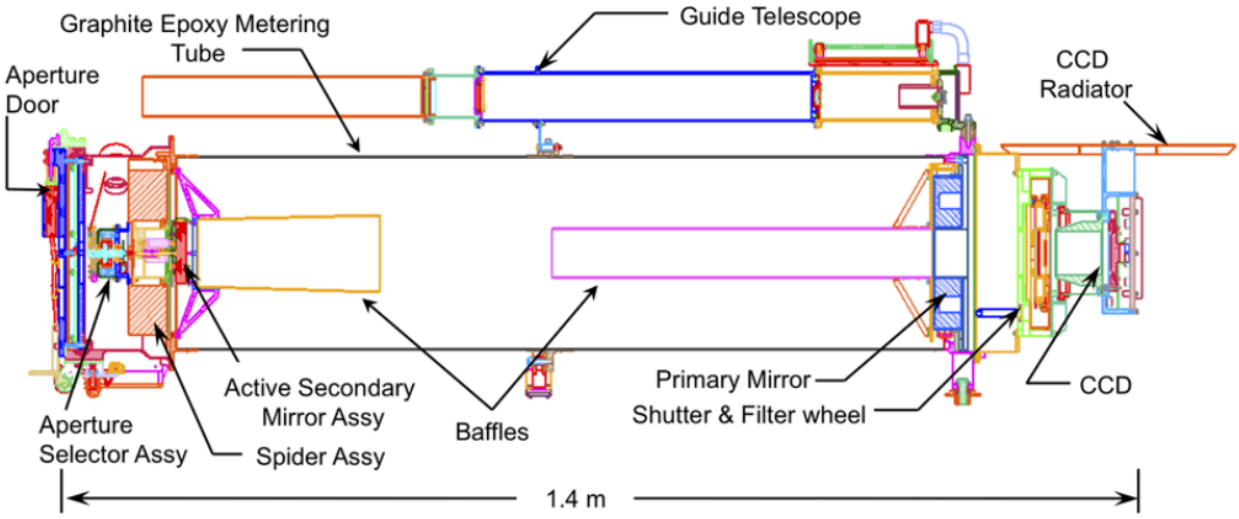

Figure 2.2: The schematic view of AIA telescope is represented. (Courtesy: Boerner *et al.* (2012))

7 Extreme Ultra-violet (EUV) and 3 Ultra-violet (UV) channels in the temperature range from 6×10^4 K to 2×10^7 K. Table 2.1 shows the observed wavelengths, corresponding ions, temperatures and observed solar regions. AIA takes Sun's observations with 12 sec temporal cadence and $1.5''$ spatial resolution. Figure 2.3 shows full disk Sun in different AIA filters.

2.2.2 Helioseismic and Magnetic Imager (HMI)

The primary scientific goals of the HMI (Scherrer *et al.*, 2012) investigation are the study of the solar dynamo process, evolution of active regions and sunspots, relation of internal activities with solar corona and heliosphere dynamics, space-weather forecasting and to understand convection zone dynamic activities. HMI instrumentation is developed by Schou *et al.* (2012). HMI onboard SDO is the first flight unit of NASA living with a star (LWS) program. HMI observes line-of-sight (LOS) magnetic flux with 45 sec cadence and vector magnetic fields with 12 min cadence in Fe I 617.3 nm photospheric spectral line with 4096×4096 pixels CCD and 0.5 arcsec per pixel resolution. It observes Doppler

Table 2.1: The AIA telescopes observe following principal ions (Courtesy: Lemen *et al.* (2012)):-

Wavelength	Principal Ions	Observed Solar Regions	Temp. (in log(T))
4500 Å	continuum	photosphere	3.7
1700 Å	continuum	temp. minimum, photosphere	3.7
304 Å	He II	chromosphere, transition region	4.7
1600 Å	C IV + continuum	transition region, upper photosphere	5.0
171 Å	Fe IX	quiet corona, upper transition region	5.8
193 Å	Fe XII, XXIV	corona and hot flare plasma	6.2, 7.3
211 Å	Fe XIV	active-region corona	6.3
335 Å	Fe XVI	active-region corona	6.4
94 Å	Fe XVIII	flaring corona	6.8
131 Å	Fe VIII, XXI	transition region, flaring corona	5.6, 7.0

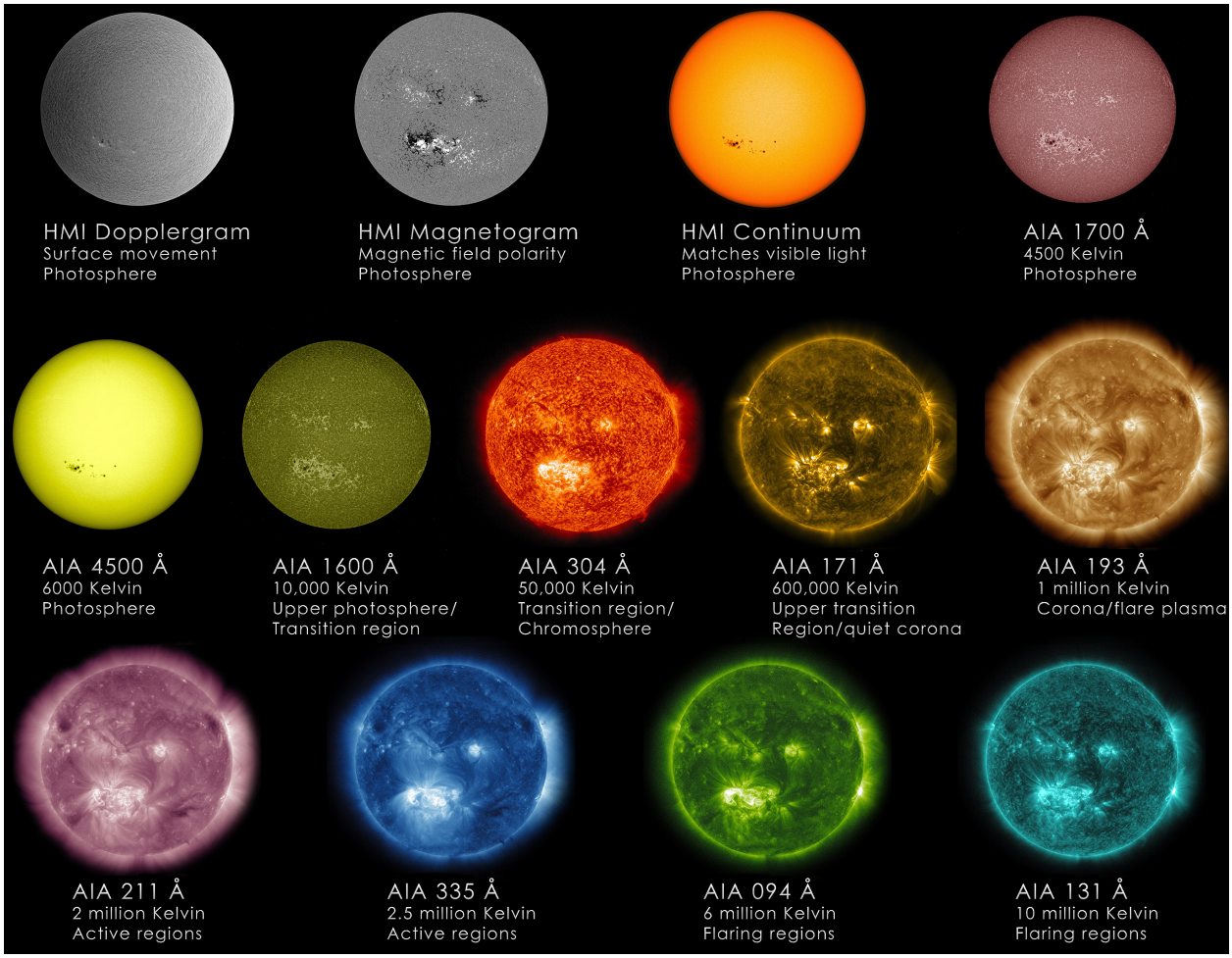

Figure 2.3: The full disk view of the Sun in different filters of Atmospheric Imaging Assembly (AIA) and Helioseismic and Magnetic Imager (HMI). (Courtesy: https://www.nasa.gov/images/content/719688main_Sun-Wavelength-Chart_full.jpg)

velocity with 1 arcsec resolution. HMI instrument is jointly developed by Lockheed Martin Solar and Astrophysics Laboratory (LMSAL) and Stanford University. To download HMI data products, one can visit Joint Science Operations Centre (JSOC) and Virtual Solar Observatory (VSO). The Virtual Solar Observatory (VSO) is a research instrument which provides solar and heliospheric physics data to the researchers and scientists. Scientists get databases for terrestrial and space-based observations there. The Joint Science Operation Center (JSOC) also provides Solar Dynamics Observatory (SDO) and other scientific mission e.g, MDI onboard SOHO, Interface Region Imaging Spectrograph (IRIS) observational data.

The instrument teams (SDO, SOHO, STEREO etc.) all provide standard processing routines, usually available through SolarSoft, and written in IDL.

2.2.3 Extreme Ultraviolet Variability Experiment (EVE)

EVE's primary objective is to measure solar EUV irradiance on solar flare timescales, recognising that variability of the EUV flux at Earth affects the Earth's ionosphere and can have impacts on satellites. The EVE (Woods *et al.*, 2012) onboard SDO measures solar Extreme Ultraviolet irradiance with 0.1 nm spectral resolution and 10 sec temporal cadence. EVE mainly includes three instruments MEGS, ESP and SAM. Multiple EUV Grating Spectrographs (MEGS)-A consists of grating spectrometers which observes solar EUV irradiance in the wavelength range from 5 to 37 nm with 2 CCDs (1024×2048) cameras. MEGS-B observes Lyman-α (121.6 nm) irradiance which is the brightest line in EUV range. The EUV SpectroPhotometer (ESP) includes series of radiometers which observes solar EUV irradiance in the wavelength range from 0.1 to 39 nm. The Solar Aspect Monitor (SAM) is the pinhole camera which provides alignment details about EVE in visible and soft X-rays wavelengths.

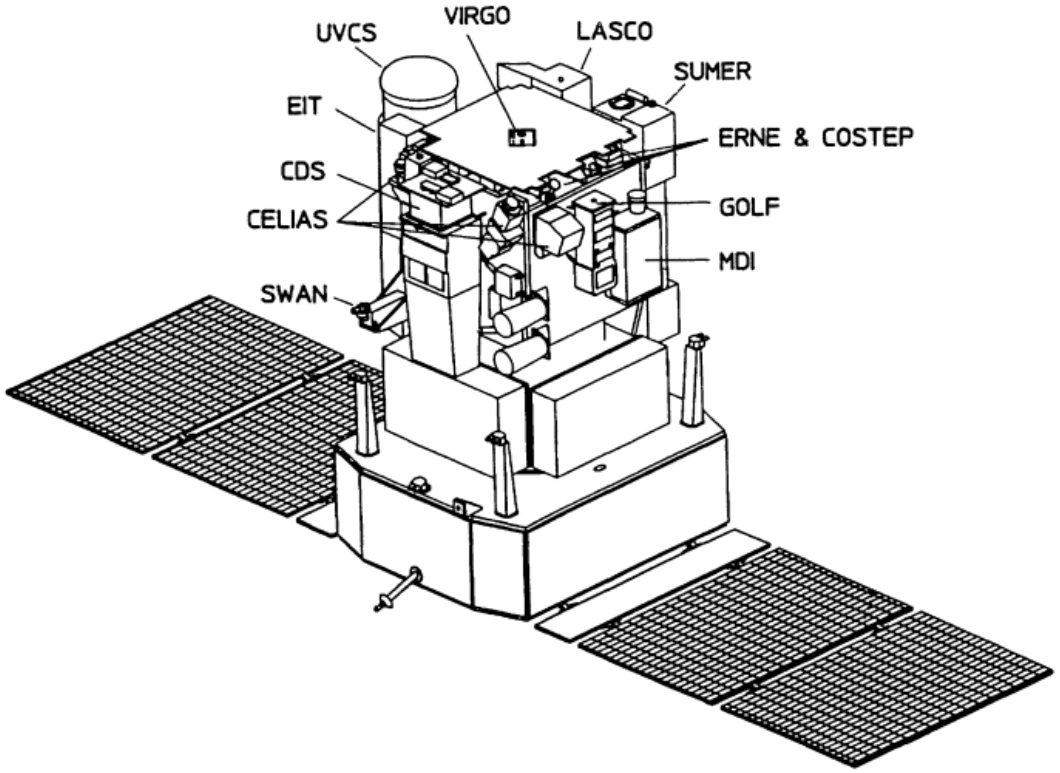

Figure 2.4: The schematic view of the SOHO mission. (Courtesy: Domingo, Fleck and Poland (1995))

2.3 Solar and Heliospheric Observatory (SOHO)

The Solar and Heliospheric Observatory (SOHO) (Domingo, Fleck and Poland, 1995) is the joint space mission of European Space Agency (ESA) and National Aeronautics and Space Administration (NASA). The primary scientific objectives of SOHO mission are to understand solar interior activity using helioseismology, coronal heating and its contribution in accelerating the solar wind. The SOHO mission includes 12 instruments which are GOLF, VIRGO, MDI/SOI, SUMER, CDS, EIT, UVCS, LASCO, SWAN, CELIAS, COSTEP, ERNE (See Figure 2.4). The Global Oscillations at Low Frequencies (GOLF), Variability of solar IRradiance and Gravity Oscillations (VIRGO) and Magnetic Doppler Imager (MDI)/Solar Oscillations Investigation (SOI) are used for helioseismology and Solar Ultraviolet Measurements of Emitted Radiation (SUMER), Coronal Diagnostic Spectrometer (CDS), Extreme-ultraviolet Imaging telescope (EIT), UltraViolet Coronagraph Spectrometer (UVCS), Large Angle and Spectrometric COranagraph (LASCO), Solar Wind ANisotropies (SWAN) are used for solar atmospheric remote sensing and Charge, ELement and Isotope ANAlysis System (CELIAS), COmprehensive SupraThermal and Energetic Partcle analyser (COSTEP) and Energetic and Relativistic Nuclei and Electron experiment (ERNE) are used for solar wind 'in situ' measurements.

In this thesis, we have used SOHO/LASCO observational data to study the CMEs.

2.3.1 Large Angle Spectroscopic Coronagraph (LASCO)

The Large Angle Spectroscopic Coronagraph (LASCO) (Brueckner *et al.*, 1995) onboard SOHO includes three coronagraphs C1, C2 and C3 which observes the solar corona from 1.1 $R_\odot$ to 30 $R_\odot$. The C1 (1.1 - 3 $R_\odot$) is internally occulted Lyot coronagraph while C2 (1.5 - 6 $R_\odot$) and C3 (3.7 - 30 $R_\odot$) are externally occulted coronagraphs. C1 was not operational after a period where SOHO was lost, in 1998. C2 and C3 are still operational. Figure 2.5 shows the optical arrangement of Lyot coronagraph. LASCO was the first space-based

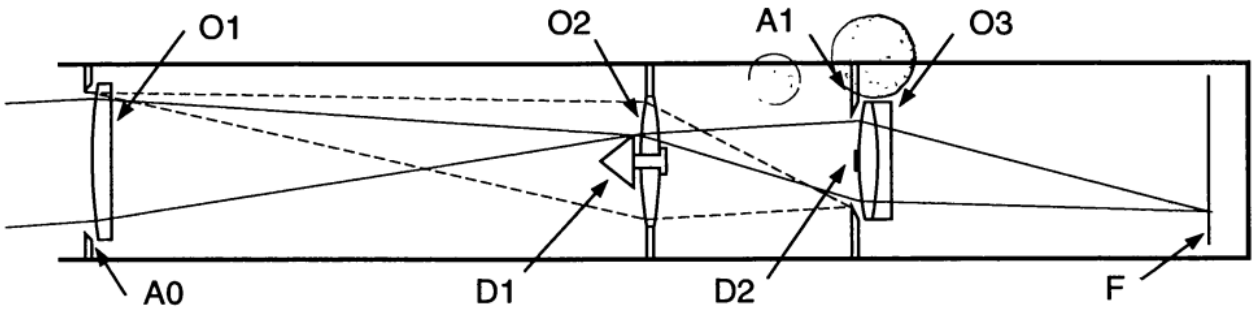

Figure 2.5: Optical arrangement of the Lyot coronagraph. In this image O1 and O3 are objective lens and O2 is a field lens. D1 is internal occulter and D2 is Lyot spot. A0 is entrance aperture, A1 is Lyot stop and F1 is the focal plane. Lyot coronagraph is developed by Lyot scientist. There is an internal occulter D1 and objective lens O1. Full disk Sun is imaged by objective lens O1 at the internal occulter. Field lens O2 captures the images of entrance aperture O1 on Lyot stop A1. Diffraction manner is also imaged by field lens O2. D2 inner occulter obstructs fake sun images which are generated by multiple reflections in O1. (Courtesy: Brueckner *et al.* (1995))

coronagraph which has spectroscopic efficiency. LASCO has 1024×1024 pixels front-side illuminated CCD camera. C1 coronagraph has a Fabry-Perot interferometer which captures full disk Sun images with 0.07 nm spectral resolution.

To study the dynamics of CMEs, we have used Coordinated Data Analysis Workshops (CDAW) automated catalog. CDAW catalog (Yashiro *et al.*, 2004) is constructed by Solar Data Analysis Center (SDAC) at the NASA Goddard Space Flight Center and Naval Research Laboratory. CDAW catalog lists all CMEs which are observed by LASCO C2 and C3 coronagraphs. In this catalog, the different parameters of CME e.g., initiation time of CME according to its appearance in LASCO C2 FOV, height, position angle and angular width are listed. To analyze the dynamics of CME, height-time parameters are fitted to first order and second order polynomial which gives constant speed and acceleration of CME respectively. All the measurements of different parameters of CMEs are done in the plane-of-sky.

2.4 Solar Terrestrial Relations Observatory (STEREO)

The Solar TErrestrial RElations Observatory (STEREO) launched on 26 October 2006 which is third mission of NASA Solar Terrestrial Probes program and it is managed by Goddard Space Flight Center (GSFC) (Driesman, Hynes and Cancro, 2008). STEREO mission consists of two observatories STEREO_A (ahead of the Earth) and STEREO_B (behind the Earth) (see Figure 2.6, Figure 2.7). STEREO_A and STEREO_B are put into the elliptical heliocentric orbits. STEREO_A and STEREO_B separate by an angle of 45° each year and preserve 1.0 ± 0.1 AU distance from the Sun. The communications with STEREO_B had lasted on 01 October 2014 but STEREO_A is still in operating mode. The major scientific tasks of STEREO are to unveil 3-D structure of CMEs and their evolution in the heliosphere, driving factors of CME initiation and triggering mechanisms of solar energetic particles in the lower coronal regions and interplanetary space. We can track a CME from Sun to Earth. Both STEREO spacecrafts consist four instruments namely the Sun Earth Connection Coronal and Heliospheric Investigation (SECCHI), the PArticles and CME Transients (IMPACT), the PLAsma and SupraThermal Ion Composition (PLASTIC) and the STEREO/WAVES (SWAVES).

In this thesis, we have used STEREO/SECCHI observational data to study the CME evolution.

2.4.1 Sun-Earth-Connection Coronal and Heliospheric Investigation (SECCHI)

The Sun Earth Connection Coronal and Heliospheric Investigation (SECCHI) has five telescope package (Howard *et al.*, 2008) which are an Extreme Ultraviolet Imager (EUVI), two Lyot coronagraphs COR1, COR2 and two Heliospheric Imagers HI-1, HI-2. All these telescopes have 2048×2048 pixels CCDs. EUVI observes chromospheric and lower

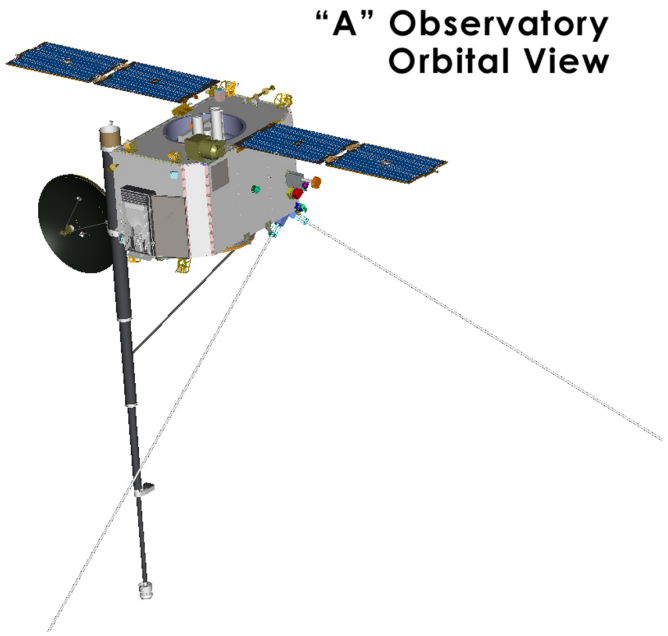

Figure 2.6: The orbital view of STEREO_A (ahead of the Earth) observatory. (Courtesy: https://stereo.jhuapl.edu/gallery/images/artistConcepts/pages/stereocloseup1.php)

coronal regions with FOV of 1-1.7 $R_{\odot}$ in four types of emission lines (He II 304 Å , Fe IX 171 Å , Fe XII 195 Å , Fe XV 284 Å) with 1.6″ pixels spatial scale. Lyot coronagraph COR1 (internally occulted coronagraph) observes inner corona from 1.5 to 4 $R_{\odot}$ and COR2 (externally occulted coronagraph) observes outer corona from 2.5 to 15 $R_{\odot}$. HI-1 observes corona from 15 to 84 $R_{\odot}$ and HI-2 observes from 66 to 318 $R_{\odot}$.

2.5 GOES Data

The Geostationary Operational Environmental Satellites (GOES) (Garcia, 1994) program is a series of geostationary satellites used for weather broadcasting, in this series 17 GOES satellites are launched till now. GOES Satellites are operated by National Oceanic and Atmospheric Administration (NOAA). GOES-1 satellite was launched on 16 October 1974 and GOES-17 satellite was launched on 01 March 2018. In the series of GOES Satellites

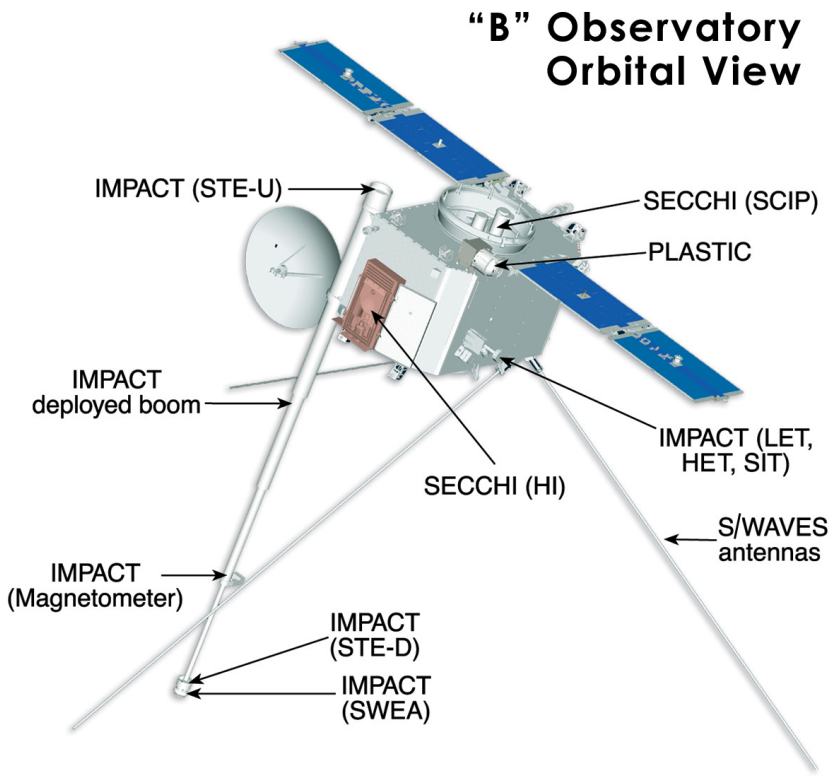

Figure 2.7: The orbital view of STEREO_B (behind the Earth) observatory. (Courtesy: https://stereo.jhuapl.edu/gallery/images/artistConcepts/pages/stereodiagram.php)

GOES-12, GOES-13, GOES-14, GOES-15 have soft X-ray imaging (SXI) capacity while GOES-16 and GOES-17 have SUVI capability. SUVI capability means it can produce full disk Sun images in EUV wavelengths by using Solar Ultraviolet Imager (SUVI). GOES 1-8 Å data are integrated. GOES Satellites observe soft X-ray fluxes in two wavelength channels 0.5-4 Å and 1-8 Å and the classification of solar flares (A, B, C, M and X-class solar flare) is based on soft channel (1-8 Å) X-ray fluxes. We have used GOES data to study emitted flux in solar flares

2.6 GONG $H\alpha$ Data

The Global Oscillation Network Group (GONG) (Harvey *et al.*, 2011) is operated by National Solar Observatory (NSO). Total six sites are operating under GONG network around the world which are Big Bear Solar Observatory, High Altitude Observatory, Learmonth Solar Observatory, Udaipur Solar Observatory, Observatorio del Teide and Cerro Tololo Interamerican Observatory. These six ground based observational sites working at different longitudinal bands and make feasible the continuous full disk observations of the Sun in 6563 Å wavelength band with one minute temporal cadence and $2''$ spatial resolution.

2.7 Hinode/X-ray Telescope (XRT) Data

The X-ray Telescope (XRT) onboard Hinode mission (Golub *et al.*, 2007) provides high spatial and temporal resolution data for study the solar corona in detail. Figure 2.8 shows XRT telescope and its different components. The primary scientific goals of the XRT are to find out the reasons of coronal heating, dynamics of solar flares and CMEs, to study magnetic reconnection and coronal jets and link between the photosphere and the corona. XRT telescope has maximum angular coverage of 34 arcmin, exposure time is ranging from 4 ms to 10 s and temporal cadence is 2s. XRT telescope observes temperature range

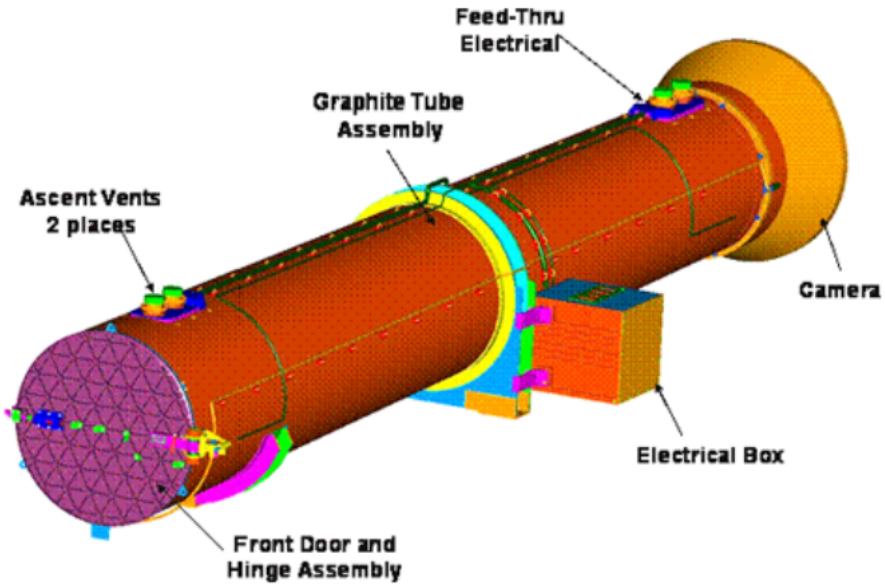

Figure 2.8: The view of XRT telescope and its different components. (Courtesy: Golub *et al.* (2007))

from 6.1 - 7.5 (in LogT). XRT telescope observes different locations of the solar corona with multi-wavelength filters with 1 arcsec per pixel angular resolution. The X-ray energy range of XRT is 0.277 keV to 2.29 keV.

2.8 Data Analysis Techniques

In the present thesis the magnetogram, EUV and H-α imaging, and coronagraphic data are used to derive various scientific results. The following analysis techniques have been used in the data analysis:

2.8.1 Calibration and Processing of the Image Data

The imaging data we obtain from SDO. These data are analyzed to understand the dynamics of coronal jets in the solar atmosphere. The raw images obtained from the CCD are flat-fielded, rebinned, processed to remove the bad pixels and spikes, and therefore, yield a clean

data. These processed images, in the form of Level 1.5 that carry physical observables, are then used for the scientific analysis. The characteristics such as number of pixels in each direction, pixel size, center coordinates are stored in the form of keywords in header of the data files. Using these keywords, the co-alignment of one or more images is performed using their image calibration routines (e.g., aia_prep.pro for SDO/AIA). This process updates these keywords of the headers in all the images corresponding to the reference image according to which all the images are aligned. It also helps us align images from different instruments having different spatial resolution. The obtained cleaned and aligned images are then enhanced by performing various operations on them. It can be resized according to the region of interests, manipulated and color contrasted for better understanding of the data. These processed image data are then subjected to various analysis described in fortcoming sub-sections.

Most of the scientific results are related with the multi-wavelength imaging observations of the jets and related eruptions, where dynamical processes are directly seen in image sequences, and magnetogram observations along with their appropriate standard analysis. We have estimated errors in some results related to the kinematics, for example, as in Figure 3.8, 3.11 and 4.15.

2.8.2 Magnetogram data and Its Analysis

The LOS magnetograms are generally operated through the same imaging processes as done for the AIA images. However, it exhibits some additional issues with the instrumental characteristics such as spatial resolution, scattered light, and filter characteristics due to the inherent complexity of the solar magnetic field at certain spatio-temporal scales. The magnetogram images are rotated and processed through hmi_prep.pro routine of SSW. We have used LOS magnetograms of SDO/HMI. SDO/HMI provides LOS magnetograms and vector magnetograms data. Even though the images are already stabilized against spacecraft

jitter by an Image Stabilization System (ISS), the manually calibrated and aligned with the reference image using 1600 Å channel of AIA to achieve the rigid co-alignment. The vector magnetograms provide three different components, e.g., field strength B_r, inclination B_θ, and azimuth B_ϕ, of the magnetic fields. Generally these parameters are used for magnetic field extrapolations to get the associated physical information in the solar atmosphere. This inversion causes the data to suffer from additional 180-degree ambiguity in the azimuthal field direction. It is first resolved using three methods: the potential-field method, the radial acute-angle method, and the random method and then subjected to the implementation of these scientific techniques for the results. In the next sub-section we depict about the PFSS technique for the magnetic field extrapolation.

2.8.3 Potential Field Source Surface (PFSS) Extrapolation

This extrapolation technique illustrates a global solar coronal magnetic field structuring on the basis of line-of-sight photospheric magnetograms taking current-free approximation into account. The global solar magnetic field is approximately radial for which current-free or non-potential field approximation can be taken. This model demonstrates the topology of solar global magnetic field by considering null point at photosphere, separatrix layers of closed and open magnetic field and different closed separatrix layers below upto the photosphere. The Global Oscillation Network Group (GONG) and Michelson Doppler Imager (MDI) synoptic magnetograms are used as a input in PFSS extrapolation method to evaluate solar coronal magnetic fields. In this thesis, we have used PFSS extrapolation code of Schrijver and De Rosa (2003) to study the coronal magnetic field topology at the time of coronal jet eruptions. The understanding of the global structure of the solar magnetic field is greatly enhanced with the help of highly efficient numerical modeling and data-driven modeling. The potential-field-source-surface (PFSS) method is one of the most generalized and simplest tools to extrapolate the coronal magnetic field in the lower

corona. The solar magnetic field in the lower corona is expected to be potential when the magnetic force dominates over all other forces. In the lower corona, the plasma β (i.e., the ratio of plasma pressure to the magnetic pressure) is low, therefore, the momentum equation is written in Priest (2014). In the lower corona, the plasma β (ratio of plasma pressure and magnetic pressure) is low, therefore, the momentum equation is written as (Priest 2014):

$$\rho \frac{\partial v}{\partial t} = -\nabla p - \nabla g + J \times B \tag{2.1}$$

The equation that considers the effects of forces from gravity, magnetic and electric forces, pressure. In the lower corona the pressure gradient and gravity is small as compared to Lorentz force, so they can be neglected. If flow speed of plasma is much less than Alfvén speed, free fall speed and sound speed, therefore LHS is put equal to zero. Therefore, only Lorentz force term survive.

$$J \times B = 0 \tag{2.2}$$

$$J = \frac{1}{\mu}(\nabla \times B) \tag{2.3}$$

Therefore current density J can be written as

$$J = \frac{1}{\mu}(\nabla \times (\nabla \times B)) \tag{2.4}$$

$$\nabla \times (\nabla \times B) = 0 \tag{2.5}$$

From equation (2.5) two conditions arise.

The first condition is,

$$\nabla \times B = 0 \tag{2.6}$$

Therefore, Magnetic field can be written in terms of gradient of a scalar field (ϕ).

$$B = -\nabla \phi \tag{2.7}$$

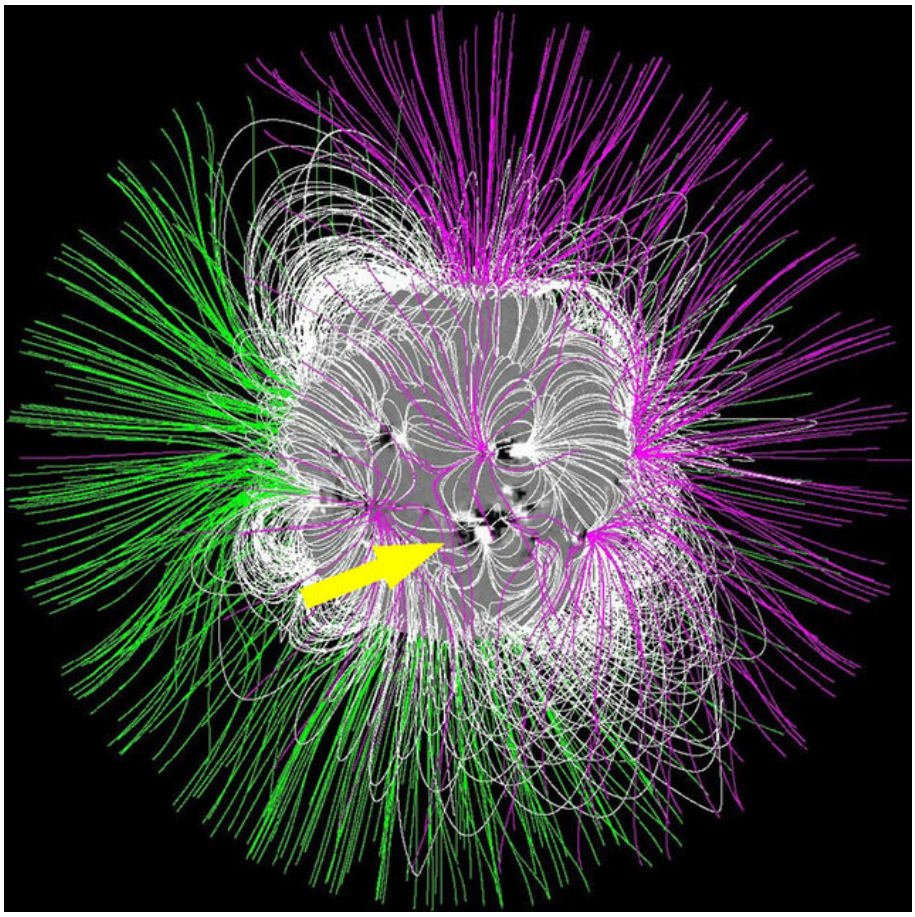

Figure 2.9: The PFSS extrapolation image has taken on 28 October 2003. The green-lines correspond to the positive polarity and the purple-lines are for negative polarity. (Courtesy: Li et al. 2011; M. De Rosa; LMSAL).

This model is known as current free or Potential free field.

Second condition or force free condition is,

$$\nabla \times B \| B \tag{2.8}$$

Current density (J) and magnetic field (B) is in same direction. Therefore Lorentz force is zero and system is known as force free region. We can write curl of magnetic field in linear terms of magnetic field, i.e.

$$\nabla \times B = \alpha B \tag{2.9}$$

Depending upon α three conditions arise,

- α=0 , System is current free or potential free and field can be written in terms of gradient of a scalar potential.
- α=(constant), System is linear force free and curl of magnetic field(B) can be written as linear combination of B.
- α depend on radial coordinate, System is non linear and known as "Non linear force free field".

$$\nabla \times B = \alpha(r) B \tag{2.10}$$

We have used potential-field-source-surface (PFSS) method in which the current density vanishes everwhere i.e. $\nabla \times B = 0$. The curl of the of equation (2.6) gives the Laplacian equation.

$$\nabla^2 B = 0 \tag{2.11}$$

In the lower corona, the magnetic field is potential, which can be written as,

$$B = -\nabla \phi \tag{2.12}$$

where ϕ is scaler magnetic potential, which satisfied the Laplace equation.

$$\nabla^2\phi = 0 \tag{2.13}$$

By solving the Laplace equation, we obtain ϕ and the corresponding magnetic field components, that satisfied $\nabla \times B = 0$ and $\nabla.B = 0$.

The standard solution of the equation (2.13) can be obtained from the use of the method of separation of variables. Using the separation of variable method for a cartesian coordinate system, we consider a 2D rectangular pipe (similar to magnetic flux tube) for which the photospheric surface is considered to be at z=0 and the solution above the XY-plane became zero as z tends to infinity having periodic solution in the x, y-direction. The boundary conditions for x,y and z directions are,

$0 \leq x \leq Ł_x$

$0 \leq y \leq Ł_y$

$0 \leq z \leq \infty$

The general solution of scalar potential of equation (2.13),

$$\Phi(x,y,z) = \sum_{m=0}^{\infty}\sum_{n=0}^{\infty} C_{m,n} exp((-\pi\sqrt{k^2+l^2})z) sin(\frac{m\pi x}{L_x}).sin(\frac{n\pi y}{L_y}) \tag{2.14}$$

and the corresponding magnetic field is

$$B(x,y,z) = -\nabla\Phi(x,y,z) \tag{2.15}$$

Gives the value $C_{m,n} = 0$ for n,m are even and $C_{m,n} = \frac{16B_0}{\pi^2 m.n}(x,y)$ if m,n are odd integer number. Thus,

$$B(x,y,z) = \frac{16B_0}{\pi^2 m.n}(x,y) \sum_{m,n=1,3,5,7,.}^{\infty} \frac{1}{mn} exp(-\pi(\sqrt{(\frac{m}{L_x})^2 + (\frac{n}{L_y})^2}z)[sinA.sinB] \tag{2.16}$$

where $A = \frac{\pi mx}{L_x}$ and $B = \frac{\pi ny}{L_y}$.

Equation (2.16) is used to extrapolate the solar magnetic field in the lower corona (1 – 2.5$R_\odot$). An example of the PFSS extrapolated global field of the coronal is shown in Figure 2.9.

We have used Potential Field Source Surface (PFSS) model to extrapolate coronal magnetic field structuring of coronal jet in Chapter 5 (ref Figure 5.9). In the lower solar corona, when magnetic force dominates over all other forces then we consider magnetic field as a potential. Here, we consider current free approximation so for this we have taken zero value for the alpha parameter. The potential field is found to be a good approximation for the large-scale coronal fields along with the jet motions can occur.

2.8.4 Fourier Local Correlation Tracking (FLCT) Technique

Fourier Local Correlation Tracking (FLCT) is a computational technique which is used to construct the velocity field/flow field in solar photospheric magnetized regions. The Local Correlation Tracking (LCT) technique is firstly introduced by November and Simon (1988) in the field of solar physics. FLCT is the fourier based local correlation technique. In this technique two maps/images I_1 (x, y, t_1) and I_2 (x, y, $t_1+\delta$t) are taken at different times where second image is at slightly later time than first image. The velocity vector is calculated. The process of calculating flow patterns goes through the different steps as in first step both images I_1 and I_2 are windowing for the interested field of view after this correlation function is calculated between these images and then find the peak location of cross correlation function. In this thesis, we have used FLCT code of Fisher and Welsch (2008) to analyse flow field at the eruption location of coronal jet by using SDO/HMI line of sight (LOS) magnetogram.

We have used Fourier local correlation tracking (FLCT) method to understand the optical plasma flow and their velocity correlation in the solar atmosphere. To obtain the 2D velocity field, two images are taken on two different times (t_1 and t_2) having intensity I_1(x,y) and I_2(x,y). The region of interest of the two images (i.e. sub-image) has been

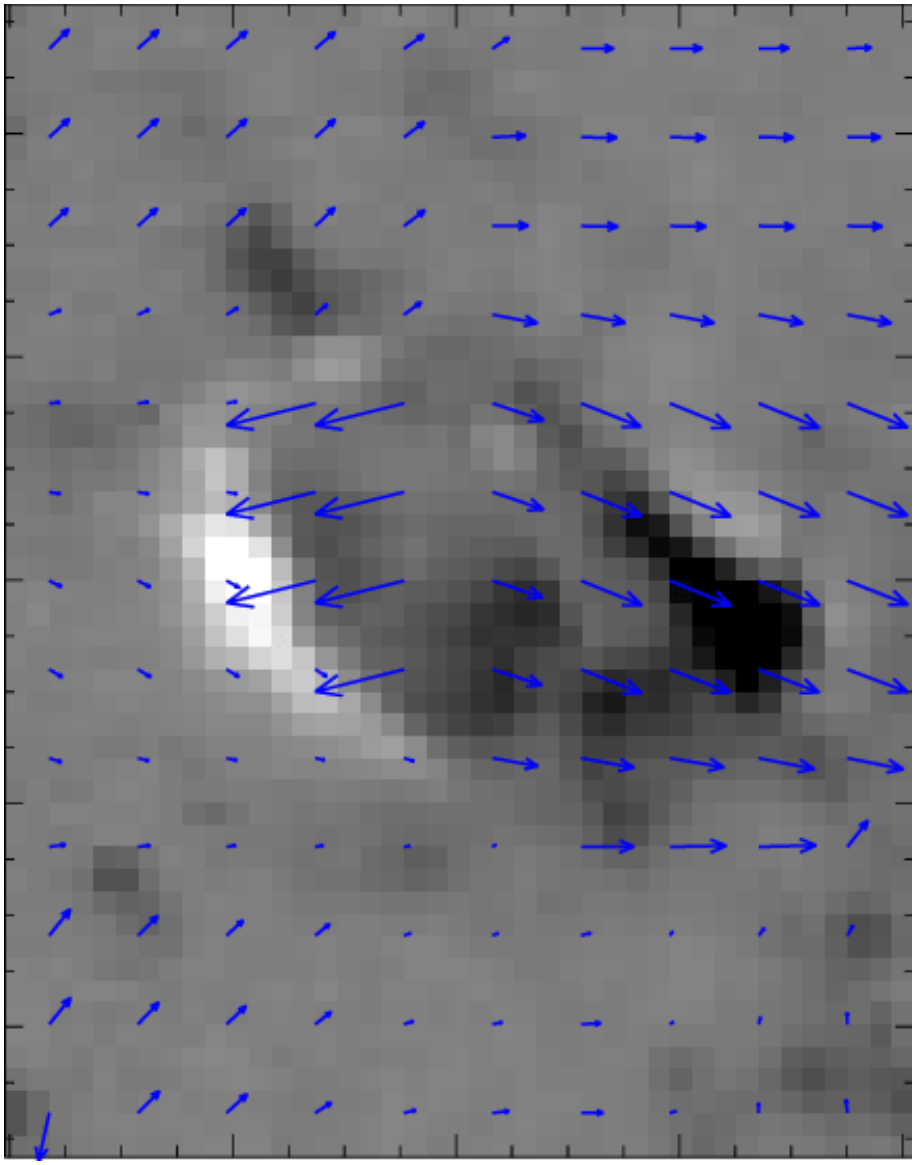

Figure 2.10: FLCT photospheric flows overplotted on MDI magnetograms on 12 February 2010. The longest arrows correspond to the flow speed of ≈335 m s^1. (Courtesy: P. Kumar)

selected by multiplying the selected images with a Gaussian width (σ) centered at the pixel locations (x_i, y_i). The sub-images can be written as,

$$S_1^{i,j}(x,y) = I_1(x,y)\frac{e^{-((x-x_i)^2+(y-y_j))^2}}{\sigma^2} \tag{2.17}$$

$$S_2^{i,j}(x,y) = I_2(x,y)\frac{e^{-((x-x_i)^2+(y-y_j))^2}}{\sigma^2} \tag{2.18}$$

In the present equations the Gaussian width (σ) is a free parameter and its most favourable value changes according to the scale size of the velocity field and nature of the selected images. The cross-correlation between two sub-images S_1 and S_2 is (Fisher and Welsh, 2008),

$$C^{i,j} = \int\int dxdy S_1^{i,j}(-x,-y)S_2^{i,j}(\delta x - x, \delta y - y) \tag{2.19}$$

where δx and δy are the shifts in the pixel locations of x_i and y_j to maximize the cross-corelation C(δx, δy) in the sub-images S_1 and S_2. The components of the velocity calculated from the FLCT: $v_x=\frac{\delta x}{\delta t}$ and $v_y=\frac{\delta y}{\delta t}$, where δt=t_2-t_1 is the time interval between two images taken on two different times.

The FLCT technique use convolution theorem to obtain the cross-correlation between two sub-images using Fourier transformation method. The Fourier transformation of two sub-images: F(S_1)=s_1(k_x, k_y) and F(S_2)=s_2(k_x, k_y).

$$C^{i,j}(x,y) = F^{-1}(S_1 * S_2) \tag{2.20}$$

where F^{-1} is inverse Fourier transfom, k_x is x-component of the wave vector, and k_y is y-component of the wave vector in Fourier space. The name of this method 'Fourier Local Correlation Tracking (FLCT)' is given due to the use of the correlation between the Fourier transform of the two sub-images. A typical exmaple of the FLCT application is shown in Figure 2.11. FLCT photospheric flows are overplotted on MDI magnetograms on 12 February 2010, in which the longest arrows correspond to the flow speed of $\approx$335 m s^{-1}. The two opposite magnetic poles are flowing apart by this maximum speed as displayed there in Figure 2.10.

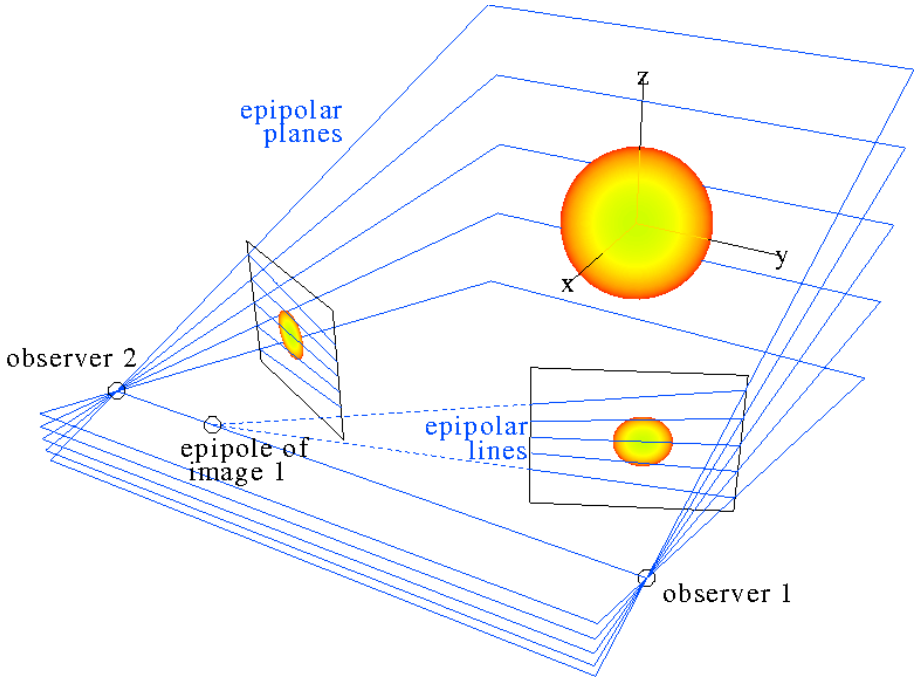

Figure 2.11: A schematic giving the overview of Tie-Pointing Method (Courtesy: B. Inhester).

2.8.5 Tie-Pointing Reconstruction Technique

Tie-Pointing Reconstruction method is a solar stereoscopic tool utilized frequently for STEREO twin satellite observations of the Sun. This technique is developed for analyzing the observational data of the STEREO mission. Here geometrical reconstruction of some object is done by detecting and recognizing this object simultaneously in two different view points. Epipolar co-ordinates are introduced for tie-pointing reconstruction. The different view-points are connected by a line which is called stereo base line that makes stereo base angle between these directions. These two view-points lie in an epipolar planes which are geometrical basis for reconstruction technique. In this thesis, we have used tie-pointing technique to observe and track the coronal jets and CMEs simultaneously in two view-points and calculate their different parameters e.g., longitude, latitude, and projected heights.

To understand the dynamical nature of coronal jets and CMEs and their 3D geometry in the solar corona, we require their exact location, height, position, etc. of a feature in the line of sight plane and in the projected plane. We select two images of the two spacecrafts with the same field of view at the same time but with widely spaced locations. The triangulation technique is used to define a plane known as the epipolar plane by taking the images from the two different spacecrafts. The epipolar plane consists of three points, two positions from two different spacecrafts, and a third point lying at the Sun's center (cf., Figure 2.11). These epipolar planes are seen along the line of sight (LOS). Therefore, these planes look like a line called as epipolar lines. The point at which these epipolar lines cut each other from two images of two spacecraft is known as tie-point. We use the tie-pointing method to obtain the real height, exact location, and position of the observed ejecta or feature by knowing the solar coordinates. The tie-pointing method use scc_measure routine written in the Interactive Data Language (IDL) available in the Solarsoft SSW library. The scc_measure routine is used to locate the position of two spacecraft as two view-points of the two observers. It takes .fits or .fts file as input and displays the two images. These .fits file contain the world coordinate system (WCS) keywords, which allow the observer to obtain the real height, exact location, and position of the features in the solar corona. A 3D reconstruction technique has been used by tracking the line of sight ray that belongs to one spacecraft and back-traced into the second spacecraft of image. The intersection of two lines (tie-point) gives the exact location and real height of the features. We have selected a point on the first image and the epipolar line that cut at tie-point shown on the other image, which passes through the same feature. This analysis is utilized for example in Chapters 3 and 4 of this thesis.

2.9 Conclusions

In this chapter, we have discussed the concept of various observational methods, related instruments, and data analysis techniques that are utilized to derive various scientific results in the present thesis. Using these techniques, detailed image analysis of the solar data (EUV and coronagraphic) has been performed to explore the physical characteristics of coronal jets and associated CMEs. Using a combination of the data from SDO, STEREO, GONG Hα, GOES, SOHO, etc., we analyze different types of coronal jets and their dynamics as well as their association with CMEs/narrow CMEs. The detailed scientific findings are discussed in Chapters 3-5. In the next Chapter 3, we describe the origin and evolution of network flare and blowout jets, and their ssociation with CMEs.